

## 5. CONCLUSIONS

In this article we have presented a design methodology for a Tx amplifier at 24 GHz using CMOS 0.13- $\mu\text{m}$  technology. Our approach provides a guideline for optimizing power and efficiency while reducing peak drain to source voltage excursions which may otherwise undermine long-term reliability. A two-stage design is presented with 19 dB small signal gain at 24 GHz. An output power of 13.6 dBm is achieved with large signal gain of 13.4 dB and 17.2% PAE. The amplifier was also evaluated for communication systems applications. At 3.8-dBm output power it produced an EVM of  $-25$  dB for an up-converted 24 GHz WLAN signal. 64-QAM OFDM signal at a data rate of 54 Mbps was used.

## ACKNOWLEDGMENTS

The authors thank Dr. J. P. Lanteri of M/A-COM Strategic Research and Development for his support of this effort. The authors acknowledge Dr. Nitin Jain of Anokiwave for designing test boards which were instrumental in the large signal amplifier characterization. Furthermore, they also thank Adil Khalil for his contribution in designing and developing differential probes which were also used in the large signal characterization of the amplifiers. Finally, they express their gratitude to Roy Bengier, Paul Roy, and Wassim Khelif for their help in the assembly and testing of the parts.

## REFERENCES

1. G. Fettweis and R. Irmer, Wireless gigabit with advances multimedia, Wireless broadband forum (WBF), 2004.
2. I. Gresham, A. Jenkins, R. Egri, C. Eswarappa, N. Kinayman, M. Jain, R. Anderson, F. Kolak, R. Wohler, S.P. Bawell, J. Bennett, and J.P. Lanteri, Ultra-wideband radar sensors for short-range vehicular applications, IEEE Trans Microwave Theory Tech 52 (2004), 2105–2122.
3. C.H. Doan, S. Emani, A.M. Niknejad, and R.W. Brodersen, Millimeter-wave CMOS design, IEEE J Solid State Circ 40 (2005), 144–155.
4. H. Shigematsu, T. Hirose, F. Brewer, and M. Rodwell, Millimeter-wave CMOS circuit design, IEEE Trans Microwave Theory Tech 53 (2005), 472–477.
5. A. Natarajan, A. Komijani, and A. Hajimiri, A fully Integrated 24-GHz phased-array transmitter in CMOS, IEEE J Solid State Circ 40 (2005), 2502–2514.
6. A. Komijani, A. Natarajan, and A. Hajimiri, A 24-GHz, +14.5-dBm fully integrated power amplifier in 0.18  $\mu\text{m}$  CMOS, IEEE J Solid State Circ 40 (2005), 1901–1908.

© 2008 Wiley Periodicals, Inc.

## THE EQUIANGULAR SPIRAL ANTENNA AT LOW FREQUENCIES

Michael McFadden and Waymond R. Scott Jr.

School of Electrical and Computer Engineering, Georgia Institute of Technology, Atlanta, GA 30332-0250; Corresponding author: m.mcfadden@gatech.edu

Received 25 June 2008

**ABSTRACT:** The effect of the geometry of the equiangular spiral antenna on the lower cutoff frequency of operation is studied using the finite-difference time-domain method. Graphs are provided that allow calculation of the cutoff frequency from the desired performance and geometry. Additionally, the patterns of the antennas at cutoff are shown. © 2008 Wiley Periodicals, Inc. Microwave Opt Technol Lett 51: 536–540, 2009; Published online in Wiley InterScience (www.interscience.wiley.com). DOI 10.1002/mop.24092

**Key words:** spiral antennas; electromagnetic analysis; broadband antennas

## 1. INTRODUCTION

Size constraints are often important when designing an equiangular spiral antenna. Some general guidelines as to how large the antenna must be to radiate at a particular frequency are available in the literature. In Dyson's original paper on the equiangular spiral, he provides a design graph that relates the geometry of the antenna to the lowest frequency at which the antenna effectively emits circularly polarized radiation [1]. This work is summarized in [2] for the self-complementary spiral with the guideline that the length of the antenna arms must exceed one wavelength,  $\lambda$ , at the lowest frequency of operation. Both studies were based on Dyson's original slot spiral and consequently do not include the effect of a substrate. In addition, each defines proper operation only in terms of the axial ratio of the antenna.

In this article, the low-frequency performance of the equiangular spiral is examined in a parametric study using a numerical model of the antenna. The lowest frequency of operation is defined in terms of three metrics: boresight axial ratio, boresight circularly polarized gain, and voltage standing wave ratio (VSWR). Graphs that show the effect of relevant antenna parameters on the lowest frequency are presented. In addition, the off-angle gain and axial ratio are examined. The parameters varied in the geometry of the spiral antenna are defined in Figure 1. There,  $R_{out}$  and  $R_{in}$  are the outer and inner truncations of the antenna.  $\psi$  is the constant angle between the radial vector and the vector tangent to the equiangular spiral curve. The substrate of the spiral is characterized by the thickness,  $t$ , and the dielectric constant,  $\epsilon_r$ . All spirals considered in this work are self-complementary. In addition, they do not include an absorbing can or ground-plane backing.

The finite-difference time-domain (FDTD) method is used to model the spirals in this work. Interested readers should consult [3] for a full description of the method and the related tools. The FDTD modeling in this study is an extension of the work in [4], where the operating-band performance of the spiral on a substrate is examined. Additional numerical modeling details may be found there.

## 2. DEFINING THE LOW-FREQUENCY CUTOFF

The equiangular spiral's lower cutoff frequency is sometimes stated to occur when the length of the arms reaches approximately

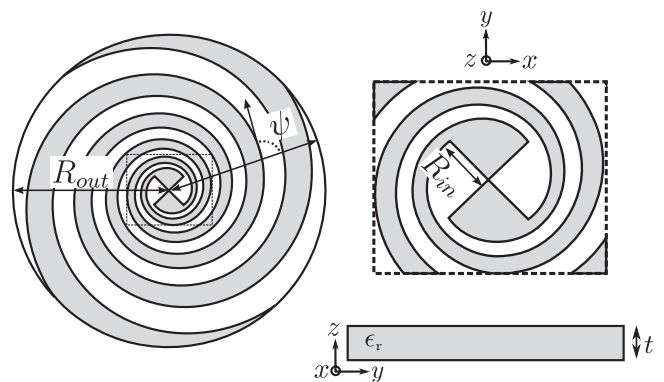


**Figure 1** Geometry of a truncated self-complementary two-arm equiangular spiral antenna on a dielectric substrate.  $R_{out}$  and  $R_{in}$  are the outer and inner truncations of the antenna.  $\psi$  is the angle between the radial vector and the vector tangent to the equiangular spiral curve. The substrate of the spiral is characterized by the thickness,  $t$ , and the dielectric constant,  $\epsilon_r$

one wavelength. The length,  $L$ , of the arms can be related to the geometry given in Figure 1 by the equation,

$$L = \sqrt{1 + (\tan\psi)^2}(R_{\text{out}} - R_{\text{in}}). \quad (1)$$

Although approximately true for smaller  $\psi$ , this guideline must fail when the spiral is tightly wrapped because  $L \rightarrow \infty$  as  $\psi \rightarrow 90^\circ$ . If the lower cutoff frequency was only a function of the length of the antenna, and not the truncation diameter, then an antenna of any size could be made to operate at an arbitrarily low frequency by wrapping the antenna tighter. An equiangular spiral curve with  $\psi$  near  $90^\circ$  closely approximates an archimedean spiral, as noted in [5]. Because the archimedean spiral has an alternative guideline for the lower cutoff frequency that is independent of the wrapping tightness, this second cutoff condition must eventually take precedence. In this article, the archimedean-style model of [6] and [7] is used as a starting point and is modified by a factor that is a function of the spiral geometry.

According to this model, the antenna's radiation primarily comes from an annular "active region" with a circumference of approximately one wavelength [8]. The design rule that is typically inferred from this model is that the antenna will operate properly when the active region fits on the spiral [6]. To be more precise, the antenna could be said to work properly at some frequency,  $f$ , when its circumference,  $C = 2\pi R_{\text{out}}$ , is larger than one wavelength, where  $\lambda = cf$  and  $c$  is the speed of light. This rule is approximately true, but there is no abrupt change in the antenna parameters when the ratio  $C/\lambda$  reaches unity. To pick a particular ratio  $C/\lambda$  that corresponds to the lower cutoff frequency, the designer must specify a definition of proper operation.

To illustrate some possibilities, the three metrics used to define proper operation in this work are shown for some typical spiral antennas in Figure 2. These include the VSWR, the boresight

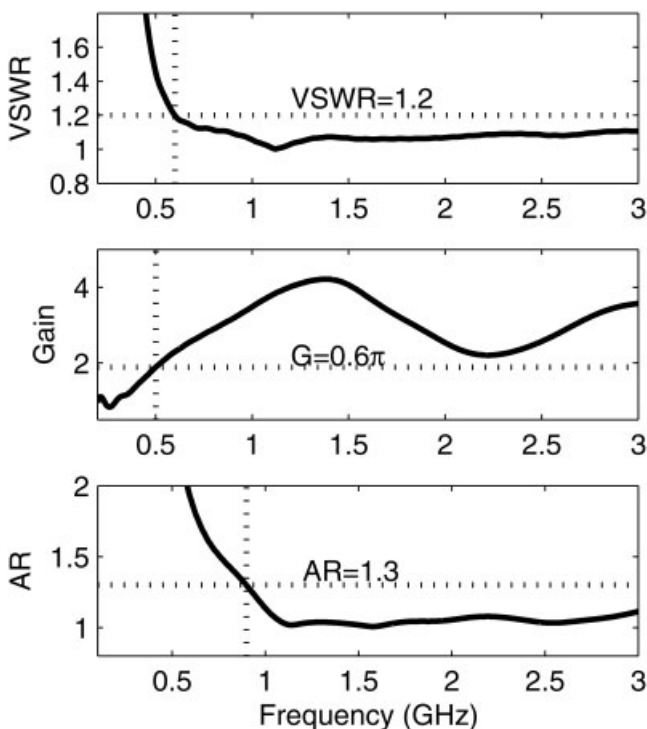


**Figure 2** Examples of the performance of the spiral antenna with the corresponding lower cutoff frequency of operation represented by a vertical dotted line

circularly polarized gain, and the boresight axial ratio. For each metric, there is a region of low frequencies where the metric has an undesirable value, and a region of higher frequencies where the metric stays relatively constant near a desirable value. The latter region of frequencies is referred to as the operating band. To determine the lower cutoff frequency of the operating band, a cutoff value is chosen that indicates the worst acceptable performance of the antenna for a given metric. The frequency that corresponds to this cutoff is taken to be the minimum frequency of operation and is shown as a vertical line on each graph in Figure 2.

To obtain the cutoff frequencies over a wide range of spiral antenna geometries, FDTD simulations for various  $R_{\text{in}}$ ,  $R_{\text{out}}$ ,  $\psi$ ,  $t$ , and  $\epsilon_r$  were run. It was found that the effect of  $R_{\text{in}}$  was negligible on the lower cutoff frequency.  $R_{\text{out}}$  had the inverse relationship to the lower cutoff frequency predicted by the active region concept. The variation of  $\psi$  was determined to be of interest for parameterization. Finally, the substrate parameters  $\epsilon_r$  and  $t$  were seen to have an erratic and usually minimal effect on the cutoff. The design graphs give the range of cutoffs associated with each dielectric simulated. Additional information on the effect of the substrate on the cutoff is provided in Section 3.

With the relevant parameters established, the ranges were determined by the available computational resources. The value of  $R_{\text{in}}$  was held constant at 7 mm. The dielectric constant,  $\epsilon_r$ , was allowed to vary from 1.0 to 6.0 in 0.5 increments. The substrate thickness,  $t$ , was held constant at 1.8 mm. The value of  $R_{\text{out}}$  was held constant at 15.24 cm. The parameter  $\psi$  was varied from  $71^\circ$  to  $82^\circ$  in  $0.5^\circ$  increments. This required 253 separate simulations of the spiral antenna. Because of its wide availability, an additional FR4 substrate with  $\epsilon_r = 4.2$  was also simulated over the same ranges.

### 3. EFFECT OF THE SUBSTRATE

Substrates that have a thicker and higher dielectric constant tend to slow the phase velocity of the currents traveling on the spiral arms when the arms are sufficiently close to one another. Because of this, a sufficiently thick substrate will reduce the wavelength for a given frequency and allow the antenna to operate at a lower frequency than it would without a substrate present. This observation is exploited to minimize the size of an archimedean spiral in [9].

The equiangular spiral, however, has the property that the distance between the spiral arms increases linearly as a function of distance from the feed. Because of this, the substrate will often have a large effect on currents near the feed, but considerably less effect near the outer truncation of the spiral. An example of this can be seen in Figure 3 where the simulated right-handed circularly polarized (RHCP) gain of a fixed spiral geometry is shown for substrate thicknesses that vary from 0 mm to an impractically thick 10 mm. Here,  $\psi = 82^\circ$ ,  $\epsilon_r = 6.0$ ,  $R_{\text{in}} = 1.4$  cm, and  $R_{\text{out}} = 15.24$  cm.

Although the thick substrates have an extremely detrimental effect in the operating band of the antenna, the lower frequencies are almost unaffected. The worst effects seen in Figure 3 occur for the substrates with electrical thicknesses that are a large fraction of a wavelength. For instance, the 10 mm substrate has an electrical thickness of  $\lambda/4$  at 3 GHz, where the response is especially erratic.

Because spirals with electrically thick substrates often do not have identifiable operating bands, this study focuses only on spirals with an electrically thin substrate. When the substrate is electrically thin, it can only have an effect on the lower cutoff frequency if the spiral is wrapped very tightly, meaning  $\psi \approx 90^\circ$ . Because the results shown in Figure 3 are for the most

tightly wrapped spirals in this study, the effect of the substrate can be ignored in this work. The minor variation because of the dielectric in the design graphs is shown as a gray band that represents the range of values over all dielectrics studied.

It may be possible to reduce the cutoff frequency of an equiangular spiral on an electrically thin substrate by wrapping it so tightly that the arm width at the truncation point is smaller than the substrate thickness. Because spirals of this type still satisfy the condition that the arm thickness varies linearly with distance from the center, they require an extremely fine resolution near the feed to be modeled properly. Spirals of this wrapping tightness could not be modeled for this study, and therefore, the results of this work should only be applied when the arm width at truncation is less than the substrate thickness.

#### 4. $C/\lambda$ RATIOS AT CUTOFF

To characterize the impedance bandwidth, a metric was desired that defines how close the impedance at a given frequency is to the operating-band impedance. To do this, the VSWR was chosen. This is the ratio of the maximum to minimum standing wave amplitude on the transmission line that feeds the antenna, and may be related to the reflection coefficient,  $\Gamma$ , by

$$\text{VSWR} = \frac{1 + |\Gamma|}{1 - |\Gamma|} \quad (2)$$

The value is always greater than one and approaches unity for a perfectly matched antenna. Because the impedance of a spiral antenna is essentially constant in its operating band, a properly driven spiral antenna will have a VSWR very near unity for a wide region of frequencies.

To generate design graphs based on the VSWR, the antennas were fed with their operating-band impedance as interpolated from a previously constructed design graph that is available in [4]. The values for  $C/\lambda$  for two different VSWR cutoff values were computed for the range of spiral antennas simulated and the results are shown in Figure 4 as a function of  $\psi$ .

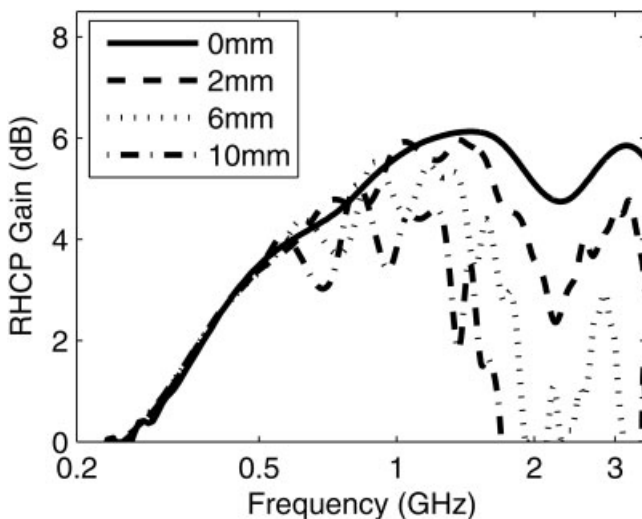


**Figure 3** Right-handed circularly polarized gain on boresight of a spiral antenna with a fixed geometry of  $\psi = 82^\circ$ ,  $\epsilon_r = 6.0$ ,  $R_{in} = 1.4$  cm,  $R_{out} = 15.24$  cm, and a varying substrate thickness. The plot shows the relatively minor effect of the substrate on the lower frequencies of operation and the degeneration of the operating band for electrically thick substrates.

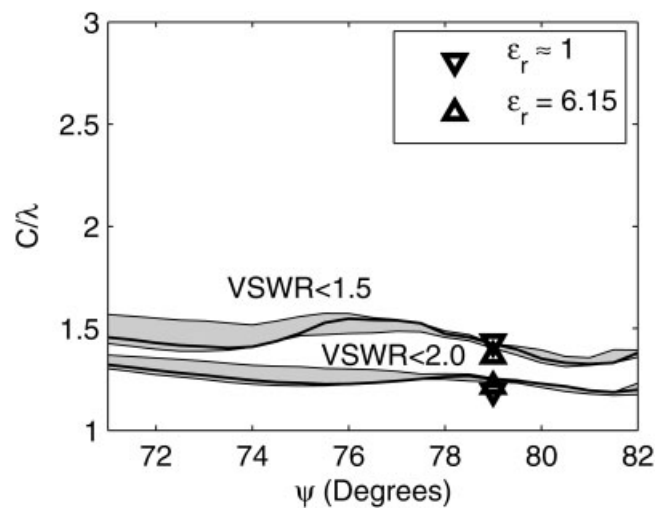


**Figure 4**  $C/\lambda$  at cutoff defined by the VSWR of the antenna as a function of  $\psi$ . The gray bands represent the range of cutoff frequencies for the substrates simulated. FR4 ( $\epsilon_r = 4.2$ ) is shown as the solid black line. Experimental data from [4] are shown as triangles for each cutoff condition.

Experimental VSWR results from [4] are included on the plot. These are for two antennas with  $\psi = 70^\circ$ ,  $R_{in} = 3$  mm, and  $R_{out} = 11.4$  cm. The substrates were chosen at the outer edges of the dielectric values in this study. A Foamclad substrate was used to emulate air, and a Rogers RO3006 substrate with  $t = 1.27$  mm and  $\epsilon_r = 6.15$  was used for the high dielectric value. The experimental results show good agreement with the simulation.

To describe the polarization properties of the antenna, the boresight axial ratio metric is used. It is defined to be the ratio of the major axis over the minor axis of the polarization ellipse. Therefore, a linearly polarized antenna will have a large axial ratio, whereas a circularly polarized antenna will have an axial ratio near unity. A plot of  $C/\lambda$  for two boresight axial-ratio cutoff values as a function  $\psi$  is shown in Figure 5.

For reference, the results of Dyson's slot-spiral bandwidth study are presented in Figure 5. Dyson's cutoff value was chosen at an axial ratio of 2.0. His  $\psi$  values range from  $65.8^\circ$  to  $78.6^\circ$ . It should be noted that his study was not restricted to self-complementary antennas. His data are given in terms of a composite parameter that he calls the angular width factor. This angular width factor is a function of  $\psi$  and a second parameter that describes the degree to which the antenna is not self-complementary. The data above  $78.6^\circ$  shown in Figure 5 were extrapolated by Dyson from non-self-complementary spirals with a  $\psi$  less than the stated value.

To describe the power radiated by the antenna, the circularly polarized boresight gain of the antenna was used as a metric. The antennas in this work radiated RHCP in the direction away from the substrate, but had the antennas been inverted, there would likely be no effect on the graphs. The RHCP gain of an antenna is defined to be the ratio of the RHCP power in a given direction radiated by the antenna to the power radiated in any direction by a perfectly isotropic radiator when each antenna is fed by a matched transmission line. This can be expressed as

$$G(\theta, \phi) = \frac{4\pi P_{RAD}}{P_{IN}} \quad (3)$$

where  $G$  is the gain,  $\theta$  is the decline from boresight,  $\phi$  is the azimuthal angle,  $P_{RAD}$  is the radiated RHCP power as a function

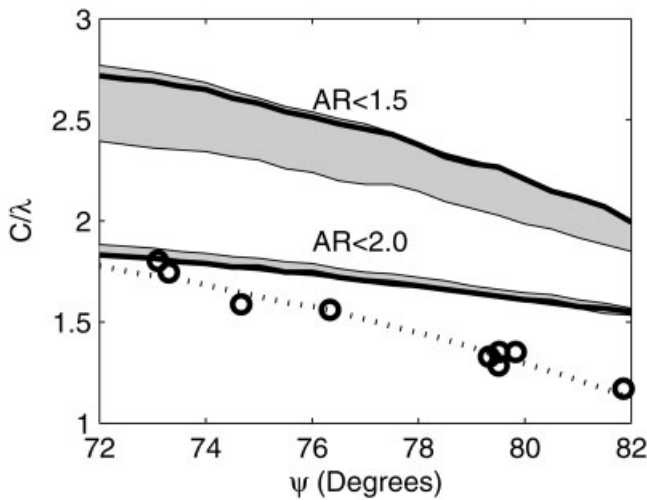


**Figure 5**  $C/\lambda$  at cutoff defined by the boresight axial ratio of the antenna as a function of  $\psi$ . The gray bands represent the range of cutoff frequencies for the substrates simulated. FR4 ( $\epsilon_r = 4.2$ ) is shown as the solid black line. The results of Dyson's slot-spiral study are shown in the dashed line. Circles mark the individual data points of his study. Note that the region above  $\psi = 78.6^\circ$  in Dyson's data is extrapolated from more loosely wrapped spirals.

of angle, and  $P_{IN}$  is the power inserted into the antenna. A plot of  $C/\lambda$  for three cutoff values of the circularly polarized gain as a function  $\psi$  is shown in Figure 6. As with the VSWR, experimental results from [4] have been included in the plot. The lowest frequency cutoff value fell below the frequency where a far-field assumption was valid in our test range and therefore only the two higher frequency cutoff bands are shown.

In Figures 4–6, one observes a general trend that increasing the parameter  $\psi$  yields a slightly better minimum frequency cutoff. This corresponds to wrapping the spiral more tightly and agrees with observations made by Dyson in [1]. The graphs also show the degree to which reducing the restriction on a given parameter allows one to reduce the size of the antenna. For instance, reducing

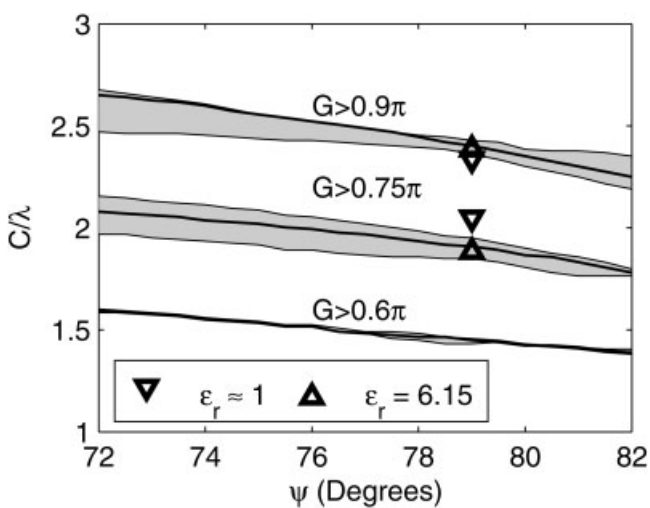


**Figure 6**  $C/\lambda$  at cutoff defined by the boresight circularly polarized gain of the antenna as a function of  $\psi$ . The gray bands represent the range of cutoff frequencies for the substrates simulated. FR4 ( $\epsilon_r = 4.2$ ) is shown as the solid black line. Experimental data from [4] are shown as triangles for the two higher frequency cutoff conditions.

the restriction on the VSWR from 1.5 to 2.0 has a negligible effect on the antenna's size, whereas reducing the restriction on the gain from  $0.9\pi$  to  $0.75\pi$  can reduce the antenna's circumference by half a wavelength at the lowest frequency of operation. As a final note, the degree to which the gray bands of the plots are thin as well as the corresponding experimental data suggest that the substrate may be ignored when calculating the lower frequency cutoff of an equiangular spiral on an electrically thin substrate for the range of  $\psi$  studied.

## 5. OFF-ANGLE PERFORMANCE

One limitation of the design graphs shown above is that the definitions of the operating band based on axial ratio and gain depend only on the boresight radiation. This was chosen because the boresight radiation tends to be the best performance for the antenna. However, in most situations, it is necessary to know the behavior of boresight as well. It was found in this work that the off-angle performance of this antenna is very stable at low frequencies.

To present this, two graphs showing the composite performance of the antenna are shown. For each antenna in the design study above, the far-field radiation in every direction at the cutoff frequency was recorded using a near-field-to-far-field transformer [3]. For the related far-field parameters, axial ratio and circularly polarized gain, a maximum and minimum value were taken over all antennas simulated. In addition, because this antenna has a great deal of rotational symmetry at low frequencies, each  $\phi$  cut was included in the minimization and maximization. The minimum and maximum values of a parameter over all  $\phi$  and  $\epsilon_r$  form the outline of a composite parameter for the antennas studied in Figures 5 and 6. In Figure 7, the composite axial ratio at cutoff is shown for each cutoff value used in Figure 5. In Figure 8, the composite gain pattern at cutoff is shown for the circularly polarized gain of the antenna given each cutoff value used in Figure 6.

Because the frequencies used in the plots were selected based on the boresight performance, each plot shows no variation at  $\theta = 0^\circ$ . On the axial ratio plots, one sees relatively little variation until near  $\theta = 50^\circ$ , where the AR varies from nearly 1 to 3. Beyond this point, the polarization becomes increasingly linear, but this region may be seen to have low relative gain from the pattern plots.

## 6. CONCLUSIONS

Design graphs showing the lower cutoff frequency of the equiangular spiral antenna over a wide region of design parameters have been shown. The general trend observed in each graph, that increasing the arm wrapping tightness tends to lead to better performance, agrees with the original work of Dyson [1]. Additionally, the graphs show that for spirals that are not wrapped extremely tightly, the substrate may be ignored when calculating the lower cutoff. The design graphs provide a quantitative correction to the standard rule for calculating the lower frequency cutoff and may

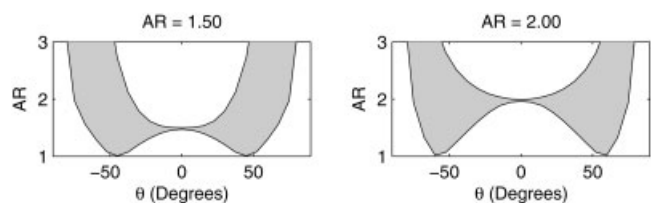


**Figure 7** The shaded region shows the composite axial ratio of the equiangular spiral antenna at the cutoff frequency. The composite contains all angles of  $\phi$  and each antenna used in the design study.

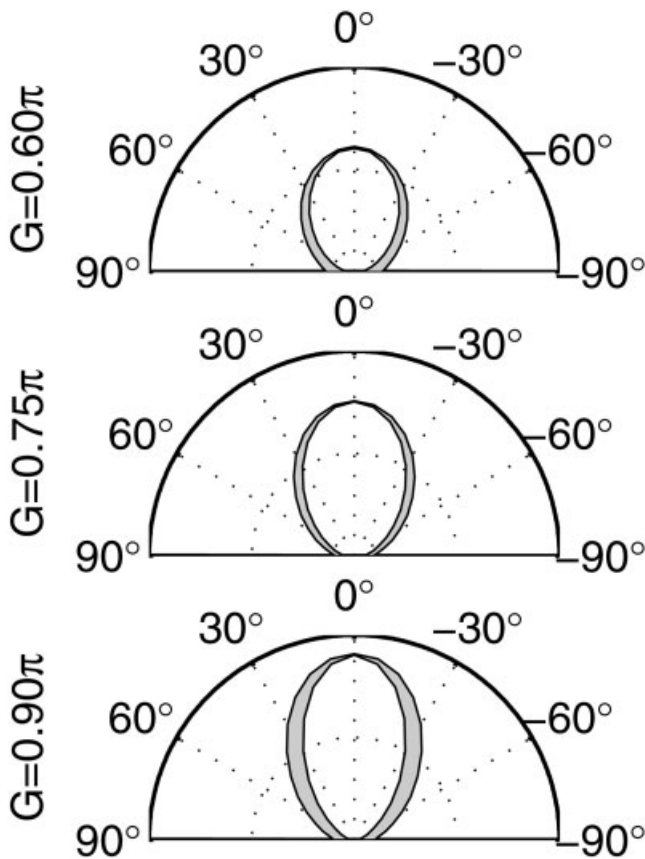


**Figure 8** The shaded region shows the composite pattern of the equiangular spiral antenna at the cutoff frequency. Composites contain all angles of  $\phi$  and each antenna used in the design study. Radial units range from 0 to  $\pi$ .

be used either to determine the minimum usable frequency of operation available for a given antenna size, or to determine the absolute minimum antenna size possible to operate at a given frequency.

This work also examines the off-angle performance of the antenna and finds it extremely well behaved with very little change observed in the shape of the pattern or off-angle axial ratio over all substrates simulated. A designer may assume that over the parameterization region given, these variables will not strongly affect the nature of the off-angle performance.

#### ACKNOWLEDGMENTS

This work was supported in part by the U.S. Army Research office under contract DAAD19-02-1-0252 and the US Army Engineer Research and Development Center Near-Surface Phenomenology Program funded under contract 912HZ-07-C-0026.

#### REFERENCES

1. J.D. Dyson, The equiangular spiral antenna, IRE Trans Antennas Propag AP-7 (1959), 181–187.
2. S.M. Wentworth and S.M. Rao, Analysis of equiangular spiral antennas, Int J Microwave Mill 6 (1996), 92–98.
3. A. Taflov and S.C. Hagness, Computational electrodynamics, 2nd ed., Artech House, Norwood, MA 2000.
4. M. McFadden and W.R. Scott, Jr., Analysis of the equiangular spiral antenna on a dielectric substrate, IEEE Trans Antennas Propag 55 (2007), 3163–3171.
5. J.D. Dyson, R. Bawer, P.E. Mayes, and J.I. Wolfe, A note on the

6. R. Bawer and J.J. Wolfe, The spiral antenna, IRE Trans Antennas Propag AP-8 (1960), 84–95.
7. R.H. DuHamel and J.P. Scherer, Antenna engineering handbook, 3rd ed., McGraw-Hill, New York, NY, 1993, Chapter 14.
8. J.A. Kaiser, The archimedean two-wire spiral antenna, IRE Trans Antennas Propag 8 (1960), 312–323.
9. B. Kramer, M. Lee, C. Chen, and J. Volakis, Design and performance of an ultrawide-band ceramic-loaded slot spiral, IEEE Trans Antennas Propag 53 (2005), 2193–2199.

© 2008 Wiley Periodicals, Inc.

## A NOVEL POLARIZATION RECONFIGURABLE RING-SLOT ANTENNA WITH FREQUENCY AGILITY

Yu-Long Zhao, Yong-Chang Jiao, Gang Zhao, Zi-Bin Weng, and Fu-Shun Zhang

National Key Laboratory of Antennas and Microwave Technology, Xidian University, Xi'an 710071, People's Republic of China; Corresponding author: faradayzhao@gmail.com

Received 3 June 2008

**ABSTRACT:** A novel reconfigurable ring-slot antenna with switchable polarization and frequency agility is presented. Circular polarization (CP) radiation of the proposed antenna is achieved by introducing proper asymmetry in the ring-slot structure and feeding the ring slot using a microstrip line at  $45^\circ$  from the introduced asymmetry. Two diodes are used to reconfigure the structure of the ring slot. Switching between right-hand and left-hand CP is achieved by turning the diodes on or off and the two CP modes are operated at different frequencies. Moreover, the antenna has a simple structure, which is easier to be fabricated. An antenna prototype is implemented and the measured results are shown. © 2008 Wiley Periodicals, Inc. Microwave Opt Technol Lett 51: 540–543, 2009; Published online in Wiley InterScience (www.interscience.wiley.com). DOI 10.1002/mop.24064

**Key words:** reconfigurable antenna; polarization diversity; circularly polarization; frequency agility; simple structure

#### 1. INTRODUCTION

Polarization diversity is attracting much attention in modern wireless communication systems. In wireless local area networks (WLAN), polarization diversity is used to alleviate the channel deterioration caused by multipath effects. Reconfigurable microstrip antennas are attractive because they can provide diversity performances to improve communication quality and capacity. Several antenna architectures, offering polarization diversity, have been reported [1–8]. In [1, 2], polarization diversity between linear polarization and LHCP/RHCP is achieved by switching the pin-diodes. In [3], two irises are orthogonal connected to a ring-slot antenna via short-length slits with each of the slits loaded by a pin diode, and the antenna can be switched back and forth between right-hand and left-hand circular polarization (CP) by turning on/off the pin diodes. In [4], a wide square slot antenna with two T-shaped metal strips connected to ground plane using pin-diodes can provide broad CP bandwidth in both RHCP and LHCP states. However, the structures of the antennas remain constant while the antenna is reconfigured; thus the two orthogonal CP modes are operated at the same frequency [3–5]. For communication systems using a frequency division multiple access technology, frequency